J. Am. Soc. Mass Spectrom. (2015) 26:716–724
DOI: 10.1007/s13361-015-1081-6

RESEARCH ARTICLE

Internal Energy Deposition for Low Energy, Femtosecond Laser Vaporization and Nanospray Post-ionization Mass Spectrometry using Thermometer Ions

Paul M. Flanigan IV,[1,2] Fengjian Shi,[1,2] Jieutonne J. Archer,[1,2] Robert J. Levis[1,2]

[1]Department of Chemistry, Temple University, 1901 N. 13th St., Philadelphia, PA 19122, USA
[2]Center for Advanced Photonics Research, Temple University, 1901 N. 13th St., Philadelphia, PA 19122, USA

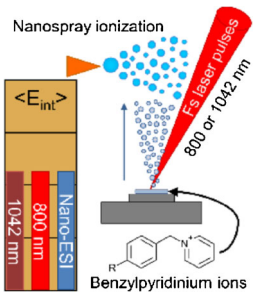

Abstract. The internal energy of p-substituted benzylpyridinium ions after laser vaporization using low energy, femtosecond duration laser pulses of wavelengths 800 and 1042 nm was determined using the survival yield method. Laser vaporization of dried benzylpyridinium ions from metal slides into a buffered nanospray with 75 μJ, 800 nm laser pulses resulted in a higher extent of fragmentation than conventional nanospray due to the presence of a two-photon resonance fragmentation pathway. Using higher energy 800 nm laser pulses (280 and 505 μJ) led to decreased survival yields for the four different dried benzylpyridinium ions. Analyzing dried thermometer ions with 46.5 μJ, 1042 nm pulse-bursts resulted in little fragmentation and mean internal energy distributions equivalent to nanospray, which is attributable to the absence of a two-photon resonance that occurs with higher energy, 800 nm laser pulses. Vaporization of thermometer ions from solution with either 800 nm or 1042 nm laser pulses resulted in comparable internal energy distributions to nanospray ionization.

Keywords: Femtosecond vaporization, Nanospray ionization, Ambient mass spectrometry, Internal energy deposition, Thermometer ions

Received: 12 May 2014/Revised: 14 January 2015/Accepted: 14 January 2015/Published Online: 28 February 2015

Introduction

Laser electrospray mass spectrometry (LEMS) [1] typically results in mass spectra with similar fragmentation patterns compared to conventional electrospray ionization-mass spectrometry (ESI-MS). In a few instances, more fragmentation was observed in LEMS analyses in comparison with conventional electrospray analysis; e.g., laser vaporization of dried irinotecan HCl [2] and dried tetrabutylammonium iodide [3] led to a greater extent of fragmentation. Conversely, LEMS has displayed less fragmentation than ESI-MS, demonstrating LEMS to be a soft vaporization technique. In one example, the folded state of aqueous lysozyme was preserved to a greater extent using LEMS in comparison with conventional ESI-MS when subjected to high collision-induced dissociation (CID) energies [4]. LEMS employs an intense (~10^{13} W/cm^2) femtosecond laser pulse to induce nonresonant vaporization of a sample. Since there is no matrix to absorb the laser energy, fragmentation may be expected with LEMS from the intense pulses; however, intact molecular ions are typically detected, as demonstrated for small biomolecules [1, 2], proteins [4–6], lipids [7], explosives [8–10], smokeless powders [11], narcotics [12], pharmaceuticals [12], and tissues [13, 14].

The internal energy distribution can be determined by measuring the fragmentation yield as a function of collision-induced dissociation energy in a series of thermometer ions via the survival yield method [15]. Thermometer ions are a set of ions that presumably acquire the same internal energy from a given mass spectral method but have different bond dissociation energies (critical energies) that vary over a suitable range for the internal energy deposited by the method [15, 16]. The key assumption of the survival yield method is that ions with an internal energy, E_{int}, below the critical energy, E_o, do not dissociate whereas all ions with an internal energy above the threshold do. This results in detection of the molecular ion when $E_{int}<E_o$ and only fragment ions when $E_{int}>E_o$. The survival yield, measuring the fraction of ions with an

Electronic supplementary material The online version of this article (doi:10.1007/s13361-015-1081-6) contains supplementary material, which is available to authorized users.

Correspondence to: Robert Levis; *e-mail:* rjlevis@temple.edu

internal energy below the dissociation threshold, can be calculated using Eq. 1,

$$SY = \frac{I(M^+)}{\left[I(M^+) + \sum I(F^+)\right]} = \int_0^{E_o} P(E)dE \qquad (1)$$

where $I(M^+)$ and $I(F^+)$ are the intensity of the molecular ion and fragment features observed in the mass spectra, respectively. Plotting each thermometer ion's survival yield as a function of its critical energy results in a sigmoidal curve, which, when differentiated, allows for the determination of the internal energy distribution, *P(E)*, of the mass analysis technique. The measured internal energy distribution represents the energetic states of the ionized analyte formed as a result of mass spectral detection.

The most common thermometer ions are substituted benzylpyridinium salts due to the relatively simple fragmentation pattern resulting from the loss of neutral pyridine, leaving the benzyl cation for mass analysis. The fragmentation pattern for the p-substituted benzylpyridinium ions is shown in Scheme 1. These molecules have well-characterized responses to the internal energy as they have similar masses, structures and degrees of freedom. Benzylpyridinium ions have been used to characterize the internal energy distributions resulting from various mass spectral methods, including: fast atom bombardment (FAB) [17], secondary ion mass spectrometry (SIMS) [18, 19], MALDI [20–22], atmospheric pressure MALDI (AP-MALDI) [20, 23], ESI [16, 24–28], desorption electrospray ionization (DESI) [29, 30], surface-assisted laser desorption/ionization (SALDI) [31], silicon nanoparticle-assisted laser desorption/ionization (SPALDI) [32], direct analysis in real time (DART) [33], surface acoustic wave nebulization (SAWN) [34], laser ablation electrospray ionization (LAESI) [35], and laser electrospray mass spectrometry (LEMS) [36].

Measurement of the internal energy distribution of dried p-substituted benzylpyridinium salts vaporized into an acidic electrospray solvent after femtosecond laser vaporization using 1.3 mJ, 800 nm laser pulses with duration of 70 fs revealed extensive fragmentation in addition to the expected benzyl cation [36]. This resulted in a higher internal energy distribution for laser vaporized dried samples in comparison to the samples analyzed with conventional ESI-MS. Two-photon excitation of the benzylpyridinium molecules was proposed as the mechanism of the enhanced fragmentation because the analytes absorb 400 nm light. Less fragmentation was observed after laser vaporization of liquid samples, with internal energy distributions similar to ESI-MS. The solvent presumably mitigated the energy transfer into the internal modes, preventing excess fragmentation.

Here, we measure the internal energy deposited during LEMS as a function of laser wavelength, pulse duration, and pulse energy using dried benzylpyridinium analytes. Experiments using 800 nm laser pulses with pulse energies of 75, 280, and 500 μJ are performed to determine the correlation between the extent of fragmentation and the intensity of the laser. In addition, thermometer ions are analyzed using 1042 nm laser pulse-bursts that are an order of magnitude longer in pulse duration to determine the internal energy deposition when using longer duration pulses and when two-photon excitation is not possible.

Experimental

Synthesis of p-Benzylpyridinium Salts

All starting materials were used as received from Sigma Aldrich (St. Louis, MO). The benzylpyridinium salts were synthesized as described [32, 34], with the reactions performed under an argon atmosphere. The methoxy- (p-MeO), methyl- (p-Me), and nitro- (p-NO_2) p-substituted benzylpyridinium salts were synthesized by mixing the respective p-benzyl chloride with an excess of anhydrous pyridine in dry acetonitrile at room temperature overnight. The p-chlorobenzylpyridinium salt (p-Cl) was prepared by heating a solution of the benzyl halide and excess pyridine in acetonitrile to 80°C for 3 hours. The salts were precipitated with diethyl ether, lyophilized, and then purified using an Xterra Prep C18 (10×150 mm, 5 μm particle) column (Waters Corporation, Milford, MA) on an Agilent 1100 series HPLC (Agilent Technologies, Inc., Santa Clara, CA). After purification, the salts were lyophilized and diluted in 1:1 (v:v) methanol/water using HPLC grade methanol (Fisher Scientific, Fair Lawn, NJ) to 1 mM stock solutions.

Sample Preparation

The stock BzPy solutions were diluted to 5 μM in 1:1 (v:v) methanol/water with 20 mM ammonium acetate for nanospray analyses. For LEMS analyses of dried and liquid samples, the stock BzPy solutions were diluted to 250 μM in 1:1 (v:v) methanol/water. For analysis of dried BzPy salts, 15 μL aliquots of the 250 μM solutions were spotted on 7×7 mm stainless steel slides and allowed to dry. This process was repeated three times, resulting in a total of 45 μL spotted on each sample slide. For analysis of liquid samples, 5 μL of the 250 μM solutions was spotted on a 2.2×3.8 cm stainless steel

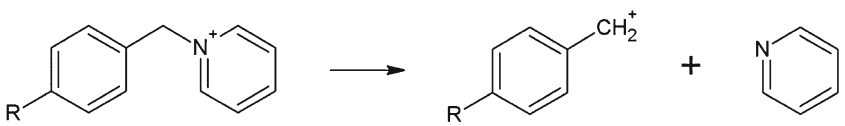

Scheme 1. Scheme of the p-substituted benzylpyridinium ion's dissociation into the benzylium cation from a neutral loss of pyridine

slide and analyzed. The nanospray solution for laser vaporization analyses was 1:1 (v:v) methanol/water with 20 mM ammonium acetate. Analyses were performed for an average of at least 15 seconds using each mass analysis method.

Laser Vaporization

Laser vaporization of the benzylpyridinium salts was performed using two different lasers. A schematic for both experimental setups is shown in Fig. 1. The 800 nm laser vaporization experiments employed laser pulses similar to those used in the previous investigation [36]. A Ti:Sapphire oscillator seeded a regenerative amplifier (both from Coherent, Inc., Santa Clara, CA, USA) to create 5 mJ, 45 fs laser pulses centered at 800 nm. The energy of the laser pulses was reduced using neutral density filters to 75, 280, and 505 μJ for vaporization of dried samples and to 280 μJ for vaporization of liquid samples. The repetition rate of the laser pulses was set at 10 Hz for analysis of fresh sample at every laser pulse. The second laser system used for vaporization was an Ytterbium-doped femtosecond fiber laser (FCPA μJewel, IMRA America, Inc., Ann Arbor, MI, USA). The fiber laser produced 50 μJ, 435 fs laser pulses centered at 1042 nm with a repetition rate of 100 kHz. Due to the high repetition rate of the laser, a two chopper system was used to reduce the rate from 100 kHz to 10 Hz pulse trains consisting of ~20 pulses with 10 μs separation. The resulting pulse train is shown as an inset in Fig. 1b. The first chopper (MC1000A, Thorlabs Inc., Newton, NJ, USA), with 9 of 10 slots covered, and the second chopper (SR540, Stanford Research Systems, Inc., Sunnyvale, CA, USA), with 29 of 30 slots covered, were set to 20 Hz and 130 Hz, respectively, to achieve the reduction in repetition rate. A quarter-wave plate and a polarizing beam splitting cube were used to attenuate the pulse energy to 46.5 μJ.

The laser beams were focused to spot sizes of ~75 μm in diameter using a 10 cm focal length lens with an incident angle of 45° with respect to the sample. The laser beams were focused 1 mm in front of the nanospray needle. The sample slides were placed on a metal plate attached to a three-dimensional translational stage (Thorlabs Inc., Newton, NJ, USA) that allowed for the sample to be raster-scanned. The metal sample holder was biased to −1245 V to correct for the distortion of the electric field.

Nanospray Post-ionization and Mass Spectrometry

After vaporization, capture and post-ionization of the analytes were performed using nanospray ionization. Nanospray-based analyses were performed using 20 μm id SilicaTip emitters (New Objective, Woburn, MA, USA) held by a conductive microtight union placed in an insulating mounting bracket (both from IDEX Health & Science, Oak Harbor, WA, USA). The nanospray needle tip, which was placed 8.25 mm from the inlet and 4.75 mm above the sample stage, was grounded and a voltage necessary to achieve stable spray (around −2.5 kV) was applied to the capillary inlet. Note that the sample stage was placed 3.75 mm under the nanospray needle in the vaporization experiments of dried benzylpyridinium ions with 800 nm pulses. The buffered nanospray solution was pumped through the needle at

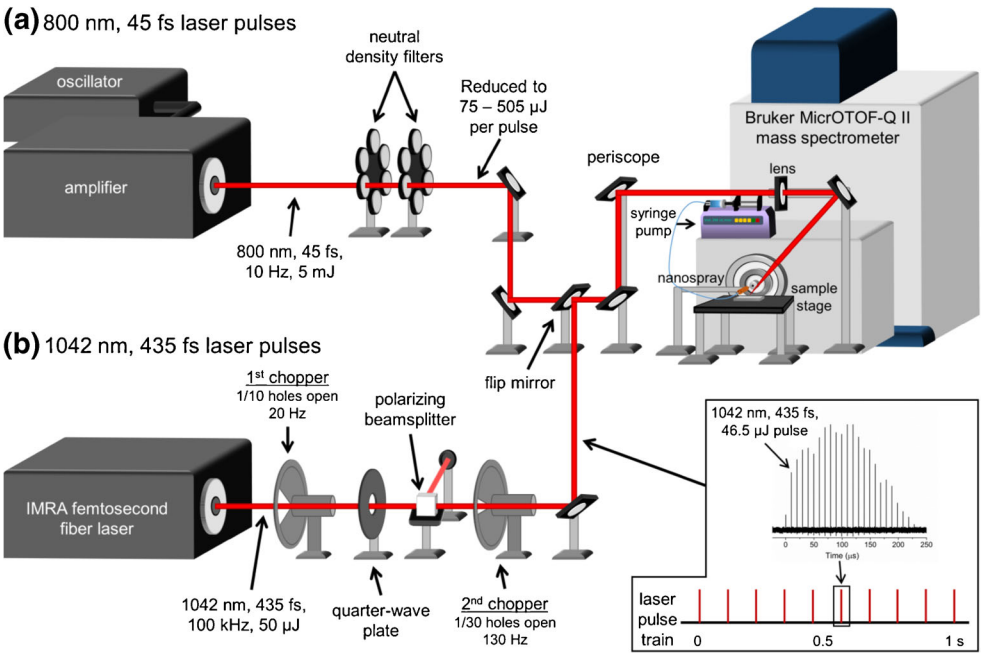

Figure 1. Schematic of the setup for the experiments using either 800 nm or 1042 nm femtosecond laser pulses for vaporization, nanospray for post-ionization, and the Bruker high resolution mass spectrometer. The pulse energy for **a**) 800 nm experiments was reduced from 5 mJ to 75 – 500 μJ by neutral density filters. The repetition rate for the **b**) fiber laser system (1042 nm, 435 fs) was reduced from 100 kHz by two choppers to 10 Hz pulse trains, each consisting of ~20 laser pulses

250 nL/min by a syringe pump (KD Scientific Inc., Holliston, MA, USA). The nanospray plume was dried before entering the inlet capillary by countercurrent nitrogen gas at 180°C flowed at 3 L/min. The high resolution mass spectrometer (Bruker MicrOTOF-Q II, Bruker Daltonics, Billerica, MA) was tuned for the range of *m/z* 50 to 500. The collision cell was set to 10 eV as it resulted in a large spread in survival yields between the p-MeO and p-NO_2 benzylpyridinium ions using conventional nanospray analysis.

Calculation of Survival Yields and Internal Energy Distributions

To verify fragment features for inclusion in the survival yield calculations, nanospray-MS/MS experiments were performed using 2 μM solutions of the benzylpyridinium salts in 1:1 (v:v) methanol/water with 20 mM ammonium acetate. The M^+ and M^+-pyridine features for the BzPy ions were isolated and fragmented using CID cell energies ranging from 2 to 45 eV. The in-source collision-induced dissociation (ISCID) voltage was adjusted to enable significant intensity of the M^+-pyridine feature for isolation and further fragmentation. The tandem MS mass spectra are shown in Figures S1 – S4 in Supplementary Material. All of the fragments verified by high resolution tandem MS (Table S1 in Supplementary Material) were used to calculate the survival yields, including those other than the M^+-pyridine ion.

The method used to calculate the internal energy distributions was based on the survival yield method [15]. The SY values for the four BzPy ions obtained at a collision cell CID voltage of 10 eV were calculated using Eq. 1 and plotted as a function of E_o. Two assumed SY values of 0% and 100% at 0 and 3.5 eV, respectively, were added to the SY curve to approximate low and high energy dissociation thresholds where complete or no fragmentation would be observed. OriginPro 9 (OriginLab Co., Northampton, MA, USA) was utilized to fit the sigmoidal curves to the experimental data points, differentiate the sigmoidal curves for the internal energy distributions and calculate the mean internal energies ($<E_{int}>$). The sigmoidal curve was fit using a Boltzmann function, as seen in Eq. 2,

$$SY = \frac{A_1 - A_2}{1 + e^{(E-E_c)/dE}} + A_2 \quad (2)$$

where E is the internal energy, E_c is the energy at the centroid of the curve, A_1 is the initial SY value, and A_2 is the final SY value. *Note that no kinetic shift correction was included in the calculations*.

Safety Considerations

Appropriate laser eye protection was worn by all lab personnel.

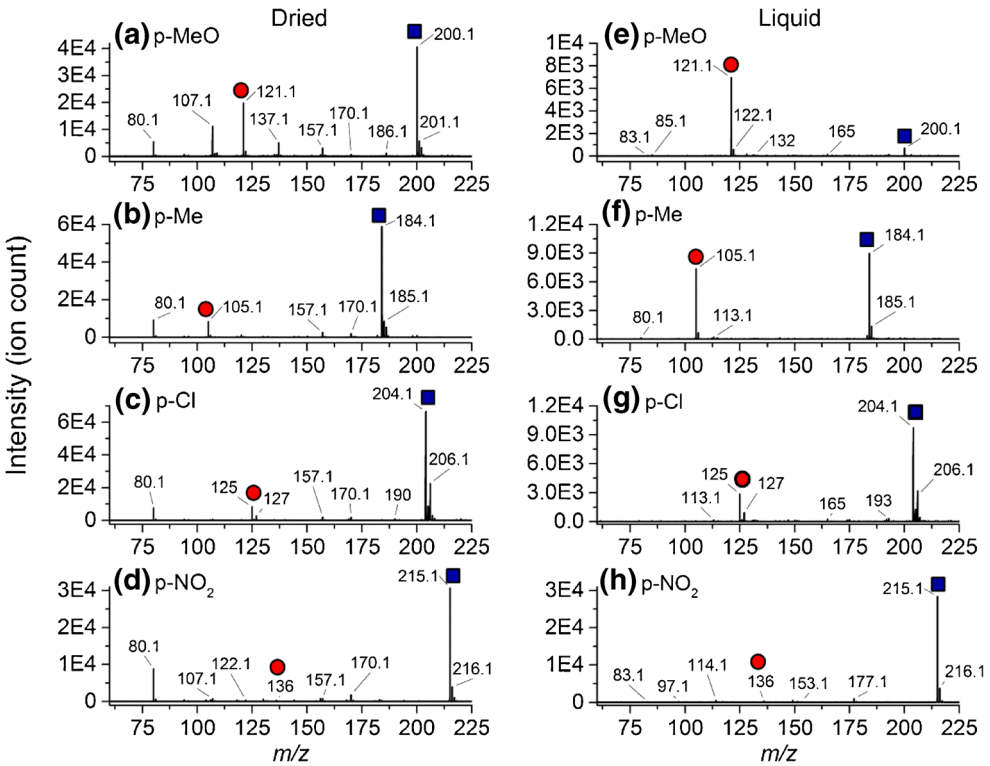

Figure 2. Blank-subtracted mass spectra for vaporization of (**a**-**d**) dried and (**e**-**h**) liquid benzylpyridinium ions using 75 μJ and 280 μJ 800 nm laser pulses, respectively, into an ammonium acetate buffered nanospray solvent for mass analysis. The M^+ and M^+-pyridine features are denoted by the blue squares and red circles, respectively

Results and Discussion

Thermometer Ion Mass Analysis using Low-Energy, 800 nm Femtosecond Laser Vaporization and Buffered Nanospray Post-ionization

Previous internal energy experiments using 1.3 mJ, 800 nm femtosecond laser pulses for vaporization of dried benzylpyridinium salts led to more fragmentation than observed with conventional ESI-MS [36]. To determine whether the extent of fragmentation could be decreased, the fragmentation distribution of the benzylpyridinium ions (p-MeO, p-Me, p-Cl, and p-NO_2 BzPy) was measured as a function of 800 nm laser vaporization energy from 75 μJ to 505 μJ. The laser vaporized material was directed into the nanospray source for post-ionization and mass spectrometry. The mass spectra for the vaporization of the dried and liquid benzylpyridinium ions with 75 μJ and 280 μJ laser pulses, respectively, are presented in Fig. 2. The *m/z* values for all features of interest are denoted on the mass spectra with the parent molecular (M^+) and parent minus pyridine (M^+-pyridine) features highlighted as blue squares and red circles, respectively. The corresponding masses and dissociation energies of the BzPy salts are shown in Table 1. As observed in the previous experiments [36], LEMS analyses of the liquid benzylpyridinium ions resulted in mass spectra similar to conventional nanospray mass spectral analysis (Fig. 3). The nanospray experiments primarily resulted in the M^+ and M^+-pyridine features with little or no other fragments. Conversely, the LEMS analyses of the dried benzylpyridinium ions resulted in several dissociation ions other than the M^+-pyridine molecule, in particular the feature at *m/z* 80.1. The ion intensity of *m/z* 80.1 increased as a function of pulse energy in the analysis of laser vaporized dried benzylpyridinium ions, as seen in the mass spectra for 280 and 505 μJ experiments (Figures S5 to S8 in Supplementary Material).

The fragments observed in these experiments have been observed previously [34, 36, 37] and presumably result from reaction pathways other than the simple loss of a neutral pyridine including intramolecular rearrangements [37] and rearrangement to the tropylium cation [28, 38, 39]. The peak at *m/z* 80.1 is assigned to $[pyridine+H^+]^+$. Note that pyridine would only be observed if the benzylpyridinium ions were already fragmented prior to entering the mass spectrometer, allowing the neutral pyridine to be charged by the nanospray solvent. The pyridine feature (*m/z* 80.1) is not observed for either conventional nanospray or femtosecond vaporization of liquid benzylpyridinium ions, but is prevalent in the analysis of dried thermometer ions. We propose that the vaporization mechanisms for dried and liquid samples are different in that excess energy is deposited into dried samples from two-photon excitation at 400 nm (Figure S9 in Supplementary Material) causing fragmentation, whereas the solvent mitigates the excited state chemistry via energy transfer to the liquid. Features other than those correlated to the M^+ and M^+-pyridine ions, such as *m/z* 80.1, 107.1, 137.1, 157.1, and 170.1, were observed in the laser vaporized dried benzylpyridinium mass spectra (Fig. 2) but not observed in the nanospray background mass spectrum (Figure S10 in Supplementary Material) and thus were also attributed as fragments of the thermometer ions. This assignment was verified by collision-induced dissociation experiments for nanospray-MS/MS of benzylpyridinium ions (Figures S1 to S4 in Supplementary Material). The fragment features used to calculate the SY values from the nanospray-MS/MS experiments are listed in Table S1.

Table 1. Dissociation critical energies and major mass spectral features expected for the benzylpyridinium ions

Analyte	E_o (eV)[a]	M^+ (*m/z*)	M^+ - Pyridine (*m/z*)
p-MeO	1.51	200.3	121.2
p-Me	1.77	184.3	105.2
p-Cl	1.90	204.7	125.6
p-NO_2	2.35	215.2	136.1

[a] Taken from reference [16]
M^+: molecular ion
E_o: critical energy

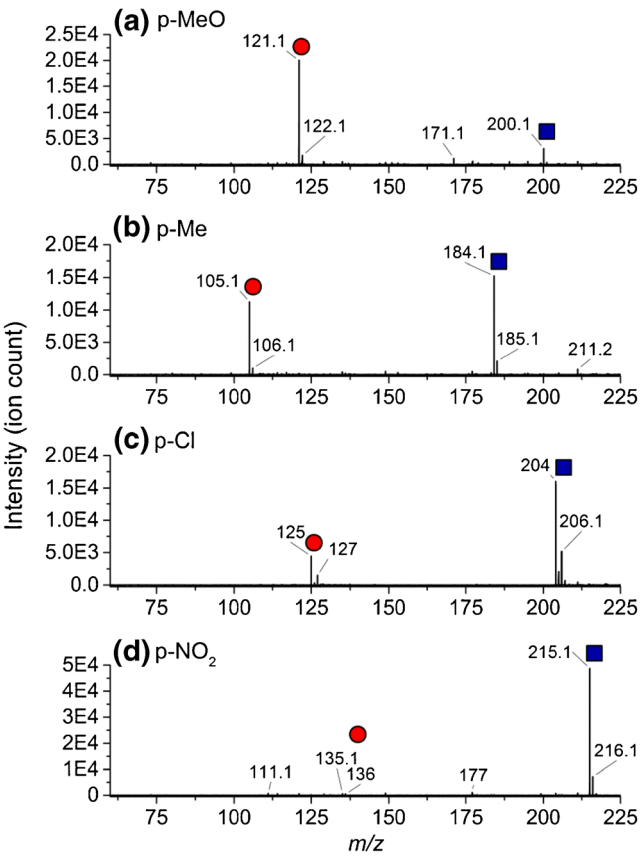

Figure 3. Blank-subtracted mass spectra of benzylpyridinium ions using nanospray with a buffered solvent. The mass spectra are labeled with the respective benzylpyridinium ion analyzed in each experiment. The M^+ and M^+-pyridine features are denoted by the blue squares and red circles, respectively

Thermometer Ion Mass Analysis using 1042 nm Femtosecond Laser Pulse-Burst Vaporization and Buffered Nanospray Post-ionization

Vaporization of benzylpyridinium ions using a fiber laser with 46.5 μJ, 435 fs laser pulses centered at 1042 nm was compared to the 800 nm measurements. The mass spectra for the fiber-laser-vaporized dried and liquid benzylpyridinium salts are shown in Fig. 4. The M^+ and M^+-pyridine distribution of the benzylpyridinium ions from fiber laser vaporization were similar to the nanospray measurements (Fig. 3). Fragment features other than M^+-pyridine were not observed except for pyridine (*m/z* 80.1) in the analysis of dried p-MeO benzylpyridinium salt, although this feature was dominated by the parent molecular and parent-pyridine ions. The pyridine feature was less prevalent when using 1042 nm laser pulse-bursts compared to 800 nm laser pulses even though the experiments with the fiber laser were performed with longer duration pulses and 20 successive pulses. This was presumably due to the lack of a two-photon resonance and an order of magnitude less intense laser pulses for the 1042 nm experiments in comparison with the 75 μJ, 800 nm experiments (2.4×10^{12} W/cm^2 vs. 3.8×10^{13} W/cm^2). These measurements demonstrate that 435 fs, 1042 nm femtosecond laser pulse-bursts were able to induce nonresonant vaporization of the ions for mass analysis similar to the 45 fs, 800 nm experiments.

Internal Energy Distributions using Low-Energy, 800 nm Femtosecond Laser Vaporization and Buffered Nanospray Post-ionization

The survival yields for the analyses of benzylpyridinium salts using laser vaporization and nanospray ionization were calculated using Eq. 1. The survival yields for nanosprayed BzPy ions and laser vaporization of liquid BzPy ions with 280 μJ pulses at 800 nm were plotted as a function of critical energy in Fig. 5. The curves were then fit with the sigmoidal function shown in Eq. 2. The sigmoidal curves resulted in excellent fits with R^2 values of 0.999 for nanospray and LEMS of liquid samples. The derivative of the sigmoidal curves yields the internal energy distributions, which are shown in Fig. 5. A summary of internal energy measurements from all experiments in this study is shown in Table 2. The resulting mean internal energies were 1.7±0.02 and 1.7±0.1 eV for nanospray and liquid LEMS analyses, respectively. We note that these internal energy measurements are not corrected by the kinetic shift of the thermometer ions within the timescale of our mass spectrometric analysis. While the uncorrected mean internal energy values may be lower than the true internal energies by a few eV, the values presented here can be used to compare the three related ionization methodologies (nanospray, dried LEMS and liquid LEMS) because the instrumental parameters are held constant between the measurements.

The sigmoidal curve for 800 nm LEMS of dried thermometer ions resulted in a poor R^2 value (Figure S11 in

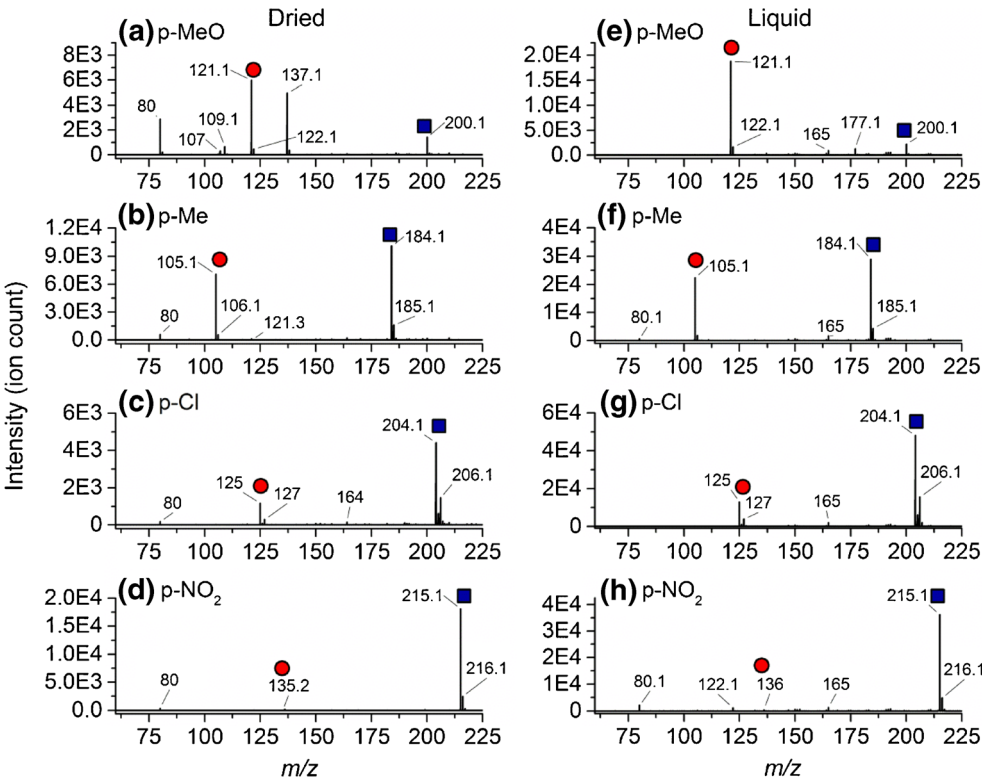

Figure 4. Blank-subtracted mass spectra using 46.5 μJ, 435 fs laser pulses centered at 1042 nm for vaporization of (**a**-**d**) dried and (**e**-**h**) liquid benzylpyridinium ions into an ammonium acetate buffered nanospray solvent for mass analysis. The M^+ and M^+-pyridine features are denoted by the blue squares and red circles, respectively

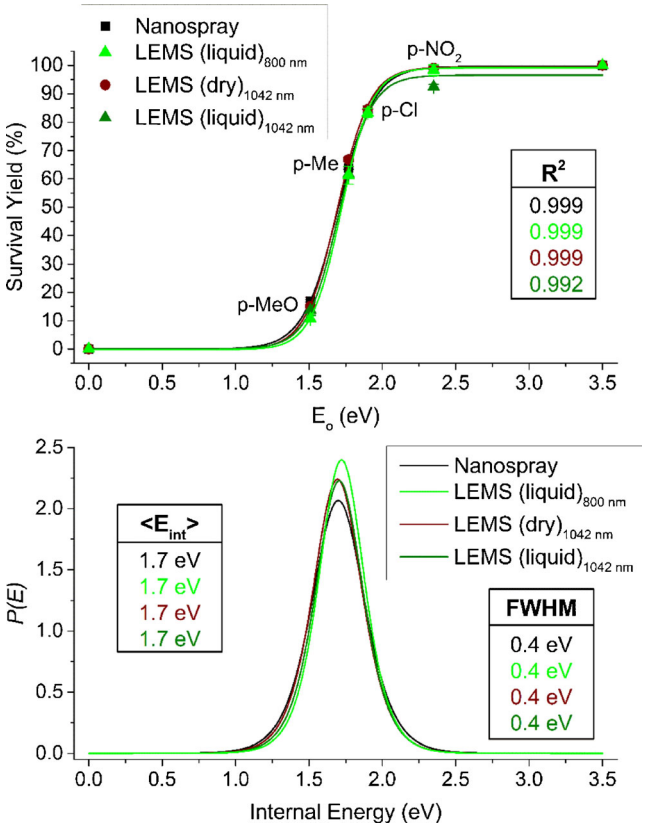

Figure 5. Internal energy deposition of LEMS using low-energy, 800 nm and 1042 nm laser pulses compared with nanospray analyses. Dried and liquid BzPy ions were vaporized into an ammonium acetate buffered nanospray solvent with 280 μJ laser pulses and 46.5 μJ for 800 nm and 1042 nm analyses, respectively. Survival yield values were plotted as a function of critical energy, E_o, at a collision cell energy of 10 eV. The derivatives of the sigmoidal curves produced the internal energy distributions (*P(E)*), as shown in the bottom plot. The sigmoidal fit R^2, $<E_{int}>$, and FWHM values for each technique are shown. Since there was no kinetic shift correction, these calculated $<E_{int}>$ values only indicate the relative internal energies

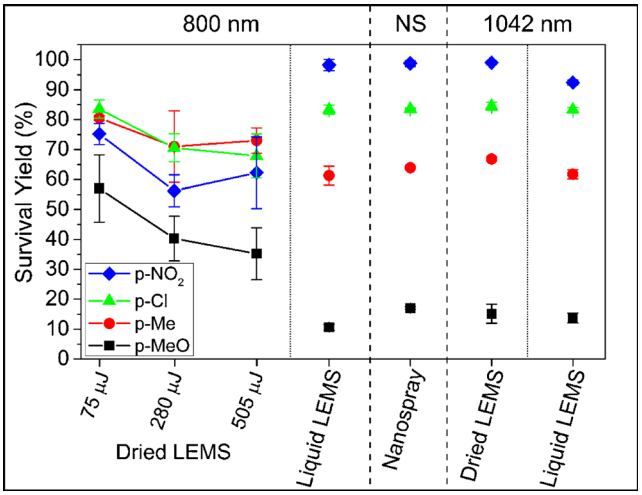

Figure 6. Comparison of survival yields of p-substituted benzylpyridinium ions for dried and liquid LEMS using 800 nm and 1042 nm pulses and liquid samples using nanospray ionization

Supplementary Material) due to the unexpected low survival yield for p-NO_2 BzPy. This is presumably caused by the two-photon excitation and fragmentation, which is supported by the large molar absorptivity at 400 nm for p-NO_2 BzPy in UV–vis experiments (Figure S9 in Supplementary Material). The two-photon fragmentation invalidates the assumption of a thermal-like energy distribution of the molecules, thereby making the model unsuitable for the calculation of the internal energy distribution of dried benzylpyridinium ions with 800 nm LEMS. To determine the effect of 800 nm pulse energies in the analysis of dried samples, the survival yield is plotted as function of pulse energy for the four BzPy ions in Fig. 6. In general, the survival yields of the benzylpyridinium ions decrease with increasing pulse energy, which is consistent with 1.3 mJ laser pulses inducing excessive fragmentation in the previous study [36]. The reduced fragmentation in the 75 μJ experiments in comparison with the 1.3 mJ study was not related to laser

Table 2. Summary of results for internal energy measurements using p-substituted benzylpyridinium salts

Wavelength	Pulse Energy	R^2 of Sigmoidal Fit	Relative $<E_{int}>$[a]	FWHM of *P(E)*
Analysis of p-substituted benzylpyridinium ions using nanospray ionization				
N/A	N/A	0.999	1.7±0.02 eV	0.4 eV
Analysis of dried p-substituted benzylpyridinium ions using laser vaporization				
800 nm	75 μJ	0.878	N/A[b]	N/A[b]
800 nm	280 μJ	0.961[c]	N/A[b]	N/A[b]
800 nm	505 μJ	0.905[c]	N/A[b]	N/A[b]
1042 nm	46.5 μJ	0.999	1.7±0.1 eV	0.4 eV
Analysis of liquid p-substituted benzylpyridinium ions using laser vaporization				
800 nm	280 μJ	0.999	1.7±0.1 eV	0.4 eV
1042 nm	46.5 μJ	0.992	1.7±0.1 eV	0.4 eV

[a] These values are relative because no kinetic shift correction was applied
[b] The SY model is not applicable for these analyses
[c] Does not include the survival yield data point for p-NO_2 in the sigmoidal fit

intensity but rather correlated to pulse energy. The laser intensity in the 75 μJ experiments was actually higher than the 1.3 mJ experiments (3.8×10^{13} W/cm^2 vs. 2.6×10^{13} W/cm^2) because the pulse duration was shorter (45 fs vs. 70 fs) and the spot size of the laser was smaller (75 μm vs. 300 μm in diameter).

The survival yields for the BzPy ions using the other laser vaporization conditions (800 nm liquid LEMS, nanospray, 1042 nm dried and liquid LEMS) are also plotted in Fig. 6 for comparison to 800 nm dried LEMS. All of the other analysis techniques had similar survival yield values, resulting in the same internal energy distributions. Analysis of dried benzylpyridinium ions using 800 nm femtosecond pulses resulted in higher survival yields for dried p-MeO and p-Me BzPy ions and lower survival yields for the dried p-NO_2 BzPy ion in comparison to the analyses with the other laser vaporization conditions. The differing survival yields for vaporization of dried and liquid samples with 800 nm, femtosecond laser pulses reaffirm the notion that the mechanisms may be different for liquid and dry LEMS. Our hypothesis is that two competing processes of two-photon absorption/fragmentation and intact vaporization affect the 800 nm dried benzylpyridinium analysis. The two-photon resonance leads to fragmentation of the benzylpyridinium ion into the pyridine fragment prior to nanospray capture (Figures S5 to S8 in Supplementary Material). In the case of aqueous vaporization, two-photon dissociation is quenched and intact vaporization is the dominant path in the vaporization mechanism, and the deposited internal energy is equivalent to nanospray ionization.

The different survival yields for laser vaporization of dried samples using 800 nm pulses could also be the result of differences in the physical properties of the vaporized neutrals in comparison with the liquid-phase analytes causing different solvation conditions and different internal energies. Also, the reported survival yields for the vaporization of dried BzPy salts may have been lessened owing to the reduced experimental timescale for fragmentation as the sample stage was 1 mm higher in comparison with the other laser vaporization measurements. Laser vaporization experiments should result in an equivalent or greater internal energy distribution than conventional nanospray ionization since the ionization method is identical in both techniques and the laser desorption process yields an additional opportunity for energy deposition. LAESI, which uses 2.94 μm, nanosecond laser pulses and nanospray post-ionization, produced similar internal energy distributions to conventional nanospray ionization in the analysis of benzylpyridinium ions [35].

Internal Energy Deposition using 1042 nm Femtosecond Laser Pulse-Burst Vaporization and Buffered Nanospray Post-ionization

The survival yields for the nanospray and fiber laser experiments were plotted as a function of critical energy in Fig. 5. The 1042 nm vaporization experiments followed the survival yield/critical energy trend observed for the nanospray measurements, resulting in R^2 values ≥0.992 for the sigmoidal curves. The internal energy distribution plot reveals that the fiber-based LEMS analyses yielded the same mean internal energy for liquid and solid samples, 1.7±0.1 eV, with similar FWHM values (~0.4 eV) as the nanospray and 800 nm liquid LEMS measurements. Using the low energy fiber laser with 435 femtosecond pulses and 1042 nm wavelength enabled "soft" vaporization of the benzylpyridinium ions even with the high repetition rate of the pulses. The results suggest that the vaporization mechanism is non-thermal because of the lack of excess fragmentation in the mass spectra. In the analysis of dried benzylpyridinium ions, desorption with fiber laser pulse-bursts resulted in the thermal-like internal energy distribution in contrast with vaporization using 800 nm pulses. The reduced fragmentation with the fiber laser is presumably due to the lack of two-photon fragmentation from the pulse-bursts at 1042 nm wavelength.

Conclusions

Femtosecond laser vaporization with low energy, 800 nm pulses or 1042 nm pulse-bursts reduced the fragmentation of dried benzylpyridinium ions observed in previous analyses with 1.3 mJ, 800 nm laser pulses. Using lower energy pulses resulted in mean internal energies comparable to or less than the conventional electrospray-based analysis methods. The absence of a two-photon resonance likely accounts for the absence of fragment features other than M^+-pyridine in the case of vaporization of dried benzylpyridinium ions with 1042 nm laser pulses. Femtosecond laser vaporization of molecules from the solution-phase led to internal energies that are comparable to, if not better than, those obtained with conventional electrospray, regardless of two-photon excitation. The differences in the fragmentation and internal energy deposition in the analysis of solid and liquid samples suggests that the femtosecond vaporization/post-ionization mechanisms are different. To obtain the "softest" analysis, liquid samples can be vaporized with 800 or 1042 nm femtosecond laser pulses at any pulse energy whereas dried samples should be desorbed with the lowest possible pulse energies, particularly if the molecule has a multiphoton resonance with the laser light.

The ability to induce soft desorption and ionization processes without any sample preparation is important for biological investigations where fragmentation may complicate the mass spectra and inhibit the identification of the parent molecule. Depositing the lowest internal energy possible during desorption enables intact molecules to be detected, which is beneficial for the analysis of peptides and proteins, lipids, tissue samples, and imaging mass spectrometry.

Acknowledgments

The authors thank Conrad Pfeiffer for the synthesis of the p-substituted benzylpyridinium salts and Andrew Mills and

Martin Fermann from IMRA America, Inc. for loan of the fiber laser. The work was supported by the Office of Naval Research (N00014-10-0293) and the National Science Foundation (CHE 0957694).

References

1. Brady, J.J., Judge, E.J., Levis, R.J.: Mass spectrometry of intact neutral macromolecules using intense non-resonant femtosecond laser vaporization with electrospray post-ionization. Rapid Commun. Mass Spectrom. **23**, 3151–3157 (2009)
2. Brady, J.J., Judge, E.J., Simon, K., Levis, R.J., Laser electrospray mass spectrometry of adsorbed molecules at atmospheric pressure. presented in part at Proc. SPIE: Imaging, Manipulation, and Analysis of Biomolecules, Cells, and Tissues VIII, San Francisco, CA, **7568**, 75680R (2010)
3. Flanigan, P.M., Perez, J.J., Karki, S., Levis, R.J.: Quantitative measurements of small molecule mixtures using laser electrospray mass spectrometry. Anal. Chem. **85**, 3629–3637 (2013)
4. Brady, J.J., Judge, E.J., Levis, R.J.: Nonresonant femtosecond laser vaporization of aqueous protein preserves folded structure. Proc. Natl. Acad. Sci. U. S. A. **108**, 12217–12222 (2011)
5. Judge, E.J., Brady, J.J., Levis, R.J.: Mass analysis of biological macromolecules at atmospheric pressure using nonresonant femtosecond laser vaporization and electrospray ionization. Anal. Chem. **82**, 10203–10207 (2010)
6. Perez, J.J., Flanigan, P.M., Karki, S., Levis, R.J.: Laser electrospray mass spectrometry minimizes ion suppression facilitating quantitative mass spectral response for multi-component mixtures of proteins. Anal. Chem. **85**, 6667–6673 (2013)
7. Brady, J.J., Judge, E.J., Levis, R.J.: Analysis of amphiphilic lipids and hydrophobic proteins using nonresonant femtosecond laser vaporization with electrospray post-ionization. J. Am. Soc. Mass Spectrom. **22**, 762–772 (2011)
8. Brady, J.J., Judge, E.J., Levis, R.J.: Identification of explosives and explosive formulations using laser electrospray mass spectrometry. Rapid Commun. Mass Spectrom. **24**, 1659–1664 (2010)
9. Flanigan, P.M., Brady, J.J., Judge, E.J., Levis, R.J.: The determination of inorganic improvised explosive device signatures using laser electrospray mass spectrometry detection with offline classification. Anal. Chem. **83**, 7115–7122 (2011)
10. Brady, J.J., Flanigan, P.M., Perez, J.J., Judge, E.J., Levis, R.J., Multidimensional detection of explosives and explosive signatures via laser electrospray mass spectrometry. presented in part at Proc. SPIE: Chemical, Biological, Radiological, Nuclear, and Explosives (CBRNE) Sensing XIII, Baltimore, MD, **8358**, 83580X (2012)
11. Perez, J.J., Flanigan, P.M., Brady, J.J., Levis, R.J.: Classification of smokeless powders using laser electrospray mass spectrometry and offline multivariate statistical analysis. Anal. Chem. **85**, 296–302 (2013)
12. Judge, E.J., Brady, J.J., Dalton, D., Levis, R.J.: Analysis of pharmaceutical compounds from glass, fabric, steel, and wood surfaces at atmospheric pressure using spatially resolved, nonresonant femtosecond laser vaporization electrospray mass spectrometry. Anal. Chem. **82**, 3231–3238 (2010)
13. Judge, E.J., Brady, J.J., Barbano, P.E., Levis, R.J.: Nonresonant femtosecond laser vaporization with electrospray postionization for ex vivo plant tissue typing using compressive linear classification. Anal. Chem. **83**, 2145–2151 (2011)
14. Flanigan, P.M., Radell, L.L., Brady, J.J., Levis, R.J.: Differentiation of eight phenotypes and discovery of potential biomarkers for a single plant organ class using laser electrospray mass spectrometry and multivariate statistical analysis. Anal. Chem. **84**, 6225–6232 (2012)
15. Kenttämaa, H.I., Cooks, R.G.: Internal energy distributions acquired through collisional activation at low and high energies. Int. J. Mass Spectrom. Ion Process. **64**, 79–83 (1985)
16. Gabelica, V., Pauw, E.D.: Internal energy and fragmentation of ions produced in electrospray sources. Mass Spectrom. Rev. **24**, 566–587 (2005)
17. Williams, D.H., Naylor, S.: The internal energy distribution in fast atom bombardment/liquid secondary ion mass spectra. J. Chem. Soc., Chem. Commun., 1408–1409 (1987)
18. Derwa, F., De Pauw, E., Natalis, P.: New basis for a method for the estimation of secondary ion internal energy distribution in 'soft'ionization techniques. Org. Mass Spectrom. **26**, 117–118 (1991)
19. De Pauw, E., Pelzer, G., Marien, J., Natalis, P. In: Ion formation from organic solids (IFOS III), ed. Benninghoven, A. Springer, pp 103–108 (1986)
20. Gabelica, V., Schulz, E., Karas, M.: Internal energy build-up in matrix-assisted laser desorption/ionization. J. Mass Spectrom. **39**, 579–593 (2004)
21. Greisch, J.F., Gabelica, V., Remacle, F., De Pauw, E.: Thermometer ions for matrix-enhanced laser desorption/ionization internal energy calibration. Rapid Commun. Mass Spectrom. **17**, 1847–1854 (2003)
22. Luo, G., Marginean, I., Vertes, A.: Internal energy of ions generated by matrix-assisted laser desorption/ionization. Anal. Chem. **74**, 6185–6190 (2002)
23. Schulz, E., Karas, M., Rosu, F., Gabelica, V.: Influence of the matrix on analyte fragmentation in atmospheric pressure MALDI. J. Am. Soc. Mass Spectrom. **17**, 1005–1013 (2006)
24. Collette, C., Drahos, L., Pauw, E.D., Vékey, K.: Comparison of the internal energy distributions of ions produced by different electrospray sources. Rapid Commun. Mass Spectrom. **12**, 1673–1678 (1998)
25. Collette, C., De Pauw, E.: Calibration of the internal energy distribution of ions produced by electrospray. Rapid Commun. Mass Spectrom. **12**, 165–170 (1998)
26. Drahos, L., Heeren, R., Collette, C., De Pauw, E., Vékey, K.: Thermal energy distribution observed in electrospray ionization. J. Mass Spectrom. **34**, 1373–1379 (1999)
27. Naban-Maillet, J., Lesage, D., Bossée, A., Gimbert, Y., Sztáray, J., Vékey, K., Tabet, J.C.: Internal energy distribution in electrospray ionization. J. Mass Spectrom. **40**, 1–8 (2005)
28. Zins, E.L., Rondeau, D., Karoyan, P., Fosse, C., Rochut, S., Pepe, C.: Investigations of the fragmentation pathways of benzylpyridinium ions under ESI/MS conditions. J. Mass Spectrom. **44**, 1668–1675 (2009)
29. Nefliu, M., Smith, J.N., Venter, A., Cooks, R.G.: Internal energy distributions in desorption electrospray ionization (DESI). J. Am. Soc. Mass Spectrom. **19**, 420–427 (2008)
30. Badu-Tawiah, A., Bland, C., Campbell, D.I., Cooks, R.G.: Non-aqueous spray solvents and solubility effects in desorption electrospray ionization. J. Am. Soc. Mass Spectrom. **21**, 572–579 (2010)
31. Tang, H.-W., Ng, K.-M., Lu, W., Che, C.-M.: Ion desorption efficiency and internal energy transfer in carbon-based surface-assisted laser desorption/ionization mass spectrometry: Desorption mechanism (s) and the design of SALDI substrates. Anal. Chem. **81**, 4720–4729 (2009)
32. Dagan, S., Hua, Y., Boday, D.J., Somogyi, A., Wysocki, R.J., Wysocki, V.H.: Internal energy deposition with silicon nanoparticle-assisted laser desorption/ionization (SPALDI) mass spectrometry. Int. J. Mass Spectrom. **283**, 200–205 (2009)
33. Harris, G.A., Hostetler, D.M., Hampton, C.Y., Fernandez, F.M.: Comparison of the internal energy deposition of direct analysis in real time and electrospray ionization time-of-flight mass spectrometry. J. Am. Soc. Mass Spectrom. **21**, 855–863 (2010)
34. Huang, Y., Yoon, S.H., Heron, S.R., Masselon, C.D., Edgar, J.S., Turecek, F., Goodlett, D.R.: Surface acoustic wave nebulization produces ions with lower internal energy than electrospray ionization. J. Am. Soc. Mass Spectrom. **23**, 1062–1070 (2012)
35. Nemes, P., Huang, H., Vertes, A.: Internal energy deposition and ion fragmentation in atmospheric-pressure mid-infrared laser ablation electrospray ionization. Phys. Chem. Chem. Phys. **14**, 2501–2507 (2012)
36. Flanigan, P.M., Shi, F., Perez, J.J., Karki, S., Pfeiffer, C., Schafmeister, C., Levis, R.: Determination of internal energy distributions of laser electrospray mass spectrometry using thermometer ions and other biomolecules. J. Am. Soc. Mass Spectrom. **25**, 1572–1582 (2014)
37. Barylyuk, K.V., Chingin, K., Balabin, R.M., Zenobi, R.: Fragmentation of benzylpyridinium "thermometer" ions and its effect on the accuracy of internal energy calibration. J. Am. Soc. Mass Spectrom. **21**, 172–177 (2010)
38. Katritzky, A.R., Watson, C.H., Dega-Szafran, Z., Eyler, J.R.: Collisionally-activated dissociation of n-alkylpyridinium cations to pyridine and alkyl cations in the gas phase. J. Am. Chem. Soc. **112**, 2471–2478 (1990)
39. Zins, E.L., Pepe, C., Rondeau, D., Rochut, S., Galland, N., Tabet, J.C.: Theoretical and experimental study of tropylium formation from substituted benzylpyridinium species. J. Mass Spectrom. **44**, 12–17 (2009)